Role of m6A RNA methylation in dosage compensation

Hemant C Naik[1‡], Runumi Baro[1‡], Amritesh Sarkar[1], Muralidhar Nayak M[2], Kartik Sunagar[2], Srimonta Gayen[1]*

[1]Chromatin, RNA and Genome (CRG) Laboratory, Department of Developmental Biology and Genetics, Indian Institute of Science, Bangalore 560012, India

[2]Evolutionary Venomics Lab, Centre for Ecological Sciences, Indian Institute of Science, Bangalore 560012, India

[‡]Equal contribution

*Correspondence: srimonta@iisc.ac.in

Abstract

In therian mammals, inactivation of one of the X-chromosomes in female cells (XX) balances the dosage of X-linked gene expression between the sexes, resulting in monoallelic expression of X-linked genes in females similar to males (XY). Therefore, it creates a dosage imbalance for X-linked genes with respect to the biallelically expressing autosomal genes (AA). X-to-autosome dosage compensation is thought to be achieved by the transcriptional upregulation of many genes from the active X-chromosome in both sexes. Here, we have delineated the role of m6A RNA methylation in the maintenance of dosage compensation in a variety of cell types, including embryonic, extra-embryonic and somatic cells. We show that m6A marks tend to be less enriched on X-linked transcripts compared to the autosomal transcripts in most of the studied cell types. However, our analysis demonstrates that m6A RNA methylation plays a minor role in dosage compensation. We show that the loss of m6A RNA methylation does not affect the maintenance of X-linked gene silencing on the inactive-X in early embryonic lineages, suggesting m6A is dispensable for the maintenance of X-chromosome inactivation. On the contrary, we show that the depletion of m6A affects X-to-autosome dosage compensation, however, the effect is minor and it occurs in a lineage-specific manner. Taken together, our study demonstrates that, although m6A marks are lowly enriched on X-linked transcripts compared to autosomal ones, it is dispensable for the maintenance of X-inactivation and has a minor contribution to the maintenance of X-to-autosome dosage compensation.

Keywords: X-chromosome upregulation, dosage compensation, m6A RNA modification, epitranscriptome, X-chromosome inactivation, Embryonic stem cells (ESCs), Epiblast stem cells.

Introduction

Mammals are characterized by a pair of sexually dimorphic chromosomes – the X and Y. However, mammalian sex is determined during the formation of zygote only by females having XX and males having XY chromosomal combinations (Charlesworth, 1991; Livernois et al., 2012). In the course of evolution, the Y-chromosome underwent massive degradation through gene-loss events (Bachtrog, 2013; Lahn & Page, 1999). This rendered male-specific monoallelic expression from single copy X-linked genes in contrast to biallelic expression from the autosomes and double copy of female X-chromosomes (Marshall Graves, 2015). Into this, Susumu Ohno hypothesised a twofold upregulation of the male X-linked gene expression to balance the X-to-autosome dosage (Ohno, 1967). Subsequently, the inheritance of this upregulated-X in females is thought to have created an overdose of X-linked gene products, which was rectified by the evolution of X-chromosome inactivation (XCI) mechanisms (Lyon, 1961). Although XCI have been investigated extensively (Gayen et al., 2015, 2016; Sarkar et al., 2015), the mere existence of X-chromosome upregulation (XCU) in mammals has been contested for decades (Deng et al., 2011; Julien et al., 2012; Kaur et al., 2020; Kharchenko et al., 2011; Xiong et al., 2010). However, recent studies leveraging allele-resolved transcriptomic analysis at the single-cell level have clearly shown coordinated upregulation of the active X-chromosome upon silencing of genes on the inactive X during early embryogenesis (Lentini et al., 2022; Naik et al., 2022). Together, while XCI balance the dosage of X-liked gene expression between sexes, X-upregulation contributes to balancing the X-to-autosome dosage. However, the mechanisms and factors involved in the maintenance of XCI and the maintenance of appropriate X-to-autosome dosage remain poorly understood. In this study, we have explored the role of N^6-methyladenosine (m6A) RNA methylation, an emerging gene regulatory player, in the maintenance of XCI and balancing the X to autosome dosage in different embryonic, extra-embryonic and somatic cell lineages.

N6-methyladenosine (m6A) is one of most prevalent internal reversible modification known to be present on RNAs (Dominissini et al., 2012; Meyer et al., 2012). Recently, m6A RNA-methylation has emerged as a new player in gene regulation, which plays key roles in embryonic development, cellular differentiation, maintenance of cellular integrity and stress response (Batista et al., 2014; Geula et al., 2015; H. Lee et al., 2019; H. B. Li et al., 2017). Dysregulation of m6A dynamics has been attributed to many pathophysiological conditions, including cancer (Berulava et al., 2020; Jiang et al., 2021; Pupak et al., 2022). m6A modification is deposited on the RNAs by the core methyltransferase complex consisting of METTL3, which is the main catalytic methylase (writer), METTL14 and WTAP, along with accessory proteins (Liu et al., 2013; Ping et al., 2014). On the other hand, FTO and ALKBH5 act as an erasure for m6A RNA modification (Jia et al., 2011; Zheng et al., 2013). Finally, the 'reader' enzymes recognize the m6A mark on the RNAs and decide their fate within a cell (Knuckles et al., 2017; Shi et al., 2017). Several studies have shown that m6A deposition occurs mostly at the 5'- and 3'-regions of transcripts and is believed to regulate translation efficiency, alternative splicing events and mRNA turnover (Ke et al., 2015; Roundtree et al., 2017; Slobodin et al., 2017; X. Wang et al., 2013, 2015; Xiao et al., 2016). Although m6A-mediated regulation is known to majorly control RNA stability, recently, it has also been shown to act as a global epigenetic regulator (Y. Li et al., 2020; Selmi & Lanzuolo, 2022; Wei et al., 2022). Together, m6A RNA methylation has emerged as one of the key players in epigenetic regulation of gene expression. Emerging studies indicate that m6A could be a critical player in regulating dosage compensation as well. However, the precise role of m6A RNA methylation in dosage compensation remains underexplored. Into that, X-inactive specific transcript or the *XIST*

lncRNA, which is the master regulator of XCI, has been shown to be highly enriched with m6A modification. Although some studies have implicated the role of m6A-regulation in *XIST*-mediated gene silencing (Chang et al., 2022; Patil et al., 2016), the essentiality of m6A in the maintenance of X-chromosome inactivation remains poorly understood. On the other hand, upregulation of the active-X has been reported at the transcriptional level through enrichment of active chromatin marks, increased chromatin accessibility and increased transcriptional burst kinetics of X-linked transcripts (Deng et al., 2013; Larsson et al., 2019; Talon et al., 2021). Given the versatile nature of m6A acting as a global epitranscriptomic regulator, it is thought that m6A-mediated regulation of transcript stabilization contributes to equilibrate the X-to-autosome dosage. However, the potential contribution of m6A in fine-tuning X-to-autosome dosage across different cell types and developmental contexts remains underexplored. In this study, we have explored the relative contribution of m6A in the maintenance of XCI as well as in maintaining an equilibrium X-to-autosome dosage in different early embryonic and extraembryonic cell types as well as in adult mouse tissues.

Results

X-chromosomal transcripts tend to harbor lower RNA m6A enrichment than autosomes.

Co-transcriptionally deposited m6A in RNA plays a significant role in regulating different biological processes. One of its prominent functions in regulating mRNA stability is thought to balance gene expression dynamics of the cells (Zaccara & Jaffrey, 2020). One of the prevailing hypotheses is that the higher stability of X-chromosomal transcripts relative to autosomal transcripts partially contributes to balance the X to autosome expression dosage in cells. However, possible factor(s) that link the higher stability of X-linked RNA to achieve a balanced X-to-autosome dosage remains underexplored. As m6A RNA methylation contributes to RNA stability, we investigated if m6A modifications are differentially enriched between X-linked and autosomal transcripts to balance the disparity between X-linked and autosomal gene expression. To explore this, we profiled the m6A enrichment on X-linked vs. autosomal transcripts in different embryonic and somatic cells using available methylated RNA immunoprecipitation sequencing (MeRIP-seq) datasets. Interestingly, we observed an overall lower enrichment of the m6A mark on X-chromosomal transcripts than the autosomal ones in cells of different early embryonic as well as GV- and MII-oocyte stages (Fig 1A). We also compared the level of m6A enrichment in transcripts between the X-linked and individual autosomes. In accordance, we observed that m6A enrichment tends to be lower in X-linked transcripts compared to most of the individual autosomes across the different embryonic and oocyte stages (Fig. 1B). Notably, we found that the enrichment of m6A level in the X-chromosomal transcripts are significantly lesser than autosomal transcripts in different mouse embryonic stem cells (ESCs) and in embryoid body (Fig. 1C). Similarly, we observed the same trend for mouse embryonic fibroblast (MEF), neural progenitor cells (NPC), immature dendritic cells (imDC), mature dendritic cells (maDC), regulatory dendritic cells (regDC), and mesenchymal stem cells (MSC) (Fig.1C). In contrast, of the three tissue types that we analyzed, difference in m6A levels was not observed in midbrain and hippocampus, however, m6A was lower on X-linked transcript compared to the autosomes, in liver tissue (Fig.1C). Taken together, we conclude that the presence of fewer m6A modifications in the X-chromosomal transcripts could play a role in its higher stability and hence regulate the X-to-autosome dosage compensation during the early embryogenesis as well as in somatic lineages.

m6A RNA methylation is dispensable for the maintenance of X-linked gene silencing in XEN, TSC and EpiSC

Next, we investigated the role of m6A RNA methylation in maintaining X-linked gene silencing on the inactive X-chromosome. For this purpose, we leveraged mouse early embryonic cell lineages that have been well established for studying XCI process. In brief, mouse undergo two waves of X-chromosome inactivation – imprinted inactivation (iXCI) of the paternal-X at the 2-4 cell stage of embryogenesis, followed by subsequent reactivation of the paternal-X in the inner cell mass cells of the late blastocyst and finally random inactivation (rXCI) of either of the paternal- or maternal-X in the embryonic epiblast (Harris et al., 2019; Maclary et al., 2014). Here, we used XEN (extra-embryonic endoderm) cells that represent the primitive endoderm of late blastocysts which have already initiated their iXCI process and thereby, maintaining the iXCI state (Fig. 2A). On the other hand, we used TSC (trophoblast stem cells) that represent the trophectodermal cells of the blastocyst and are in a maintenance phase of iXCI (Fig. 2A). Apart from these two, we used EpiSC (epiblast stem cells) lines resembling much of post-implantation epiblast in which the cells have exited the initiation of rXCI and entered into the maintenance phase (Fig. 2A). While XEN and TSC give rise to extra-embryonic lineages, EpiSC cells are representative of the embryonic lineage. Hence, these developmental cell lineages were ideal model systems to study the functional role of m6A in the maintenance of X-linked gene silencing, representing both imprinted- and random X-chromosome inactivation. Notably, all are hybrid cell lines carrying polymorphic X-chromosomes (X^{Mus}: *Mus musculus* origin and X^{Mol}: *Mus molossinus* origin), which allowed us to differentiate the X-linked gene expression from the active- vs. inactive-X through allele-specific expression analysis of X-linked genes (Fig. 3A). To investigate the role of m6A in the maintenance of X-inactivation, we depleted m6A in XEN, TSC and EpiSC through inhibition of m6A methyl transferase METTL3 using STM2457 inhibitor (Yankova et al., 2021) (Fig. 2A). Next, to validate the m6A depletion upon inhibition of METTL3, we performed liquid chromatography- tandem mass spectrometry (LC-MS/MS) to quantitate m6A levels in mRNAs isolated from DMSO treated and inhibitor (STM2457) treated XEN, TSC and EpiSC cells. We observed considerable m6A depletion upon inhibition of METTL3 (XEN, n=3; EpiSC and TSC, n=2) (Fig. 2B). Notably, in the inhibitor-treated cells, we observed a 76.5% reduction of m6A/A levels in XEN, 75.5% in TSC and 70% in EpiSC cells compared to vehicle control. Subsequently, to profile the status of X-linked gene silencing upon global m6A depletion, we performed a chromosome-wide expression analysis of all the X-linked genes in XEN, TSC and EpiSC at an allelic resolution (Fig. 3A). Of note, in all our cell lines, the X^{Mus} is selectively inactivated, which allowed us to disentangle the X-linked gene expression between active vs. inactive X through allele-specific analysis. As expected, we observed majority of the X-linked genes present on the inactive-X (X^{Mus}) remained silenced in the DMSO treated XEN, TSC and EpiSC (Fig. 3B). Only a few genes showed constitutive biallelic expression which are known escapees of XCI (Berletch et al., 2011) (Fig. 3B). Surprisingly, we observed absolutely no signs of reactivation of inactivated genes upon m6A depletion through our allele-specific RNA-seq analysis in the inhibitor-treated XEN, TSC and EpiSC cells (Fig. 3B). Overall, our analysis suggests that m6A RNA methylation is dispensable for maintaining the X-linked gene silencing in female XEN, TSC and EpiSC cells.

Depletion of m6A RNA methylation affects X to autosome dosage compensation

Next, we were curious to know if m6A RNA methylation contributes to maintaining the X to autosome dosage compensation as m6A were differentially enriched between X-linked vs. autosomal transcripts (Fig. 1). It is believed that while less enrichment of m6A on X-linked transcripts increase their stability, higher enrichment on autosomal transcripts reduces the stability of autosomal RNAs and thereby partly contribute to the maintenance of the X to autosome dosage equilibrium. Therefore, we hypothesized that the depletion of m6A might perturb the X to autosome dosage equilibrium. To test our hypothesis, we compared the allelic X to autosome expression ratio, specifically the active-X^{Mol}:A^{Mol} ratio between vehicle and inhibitor treated (m6A-depleted) XEN, TSC and EpiSC cells. As expected, we found that active-X^{Mol}:A^{Mol} ratio in vehicle treated XEN, TSC and EpiSC was ~2, indicating upregulation of X-linked gene expression from the active-X chromosome. Interestingly, we found that depletion of m6A RNA methylation in XEN, TSC and EpiSC resulted in a slight downward shift in the active-X^{Mol}:A^{Mol} ratio compared to vehicle (Fig. 4A). However, reduction in active-X^{Mol}:A^{Mol} ratio was not significant in XEN and TSC in contrast to EpiSC. To test further, we compared the overall expression of autosomal and X-linked genes between vehicle vs. m6A-depleted XEN, TSC and EpiSC at an allelic resolution. We observed that expression of X-linked genes from the active-X was significantly higher compared to the autosomal allelic expression in DMSO treated XEN, TSC and EpiSC, corroborating the upregulation of X-linked gene expression, which was maintained in inhibitor-treated cells despite the depletion of m6A RNA methylation (Fig 4A). Next, we tested if there were overall changes in allele-wise expression of X-linked and autosomal genes between DMSO vs. inhibitor-treated cells. Surprisingly, we did not observe any significant changes in expression of X-linked genes on the active-X chromosome between DMSO vs. inhibitor treated cells (Fig 4A). However, we found significant changes of autosomal allelic expression between DMSO and inhibitor treated cells (Fig 4A). Notably, the autosomal expression was tended to be increased in inhibitor treated TSC and EpiSC cells (Fig 4A). Taken together, we conclude that depletion of m6A RNA methylation has a minor impact on X-to-autosome dosage equilibrium in XEN, TSC and EpiSC.

Next, we extended our investigation to test whether m6A depletion perturbs the overall X to autosome dosage equilibrium in other cell types. We compared the X:A ratio in wild-type (WT) vs. m6A-depleted Mettl3 knockout (KO) or knockdown (KD) ESCs, maDCs, MSCs, 3T3-L1 MEFs, brain and mouse liver cells (Duda et al., 2021; Geula et al., 2015; C.-X. Wang et al., 2018; H. Wang et al., 2019; S. Wang et al., 2023; Wu et al., 2018; Xu et al., 2021; Zhao et al., 2014). Surprisingly, we found no significant changes in X:A ratio in most of the m6A-depleted cell types (Fig. 4B). However, we observed a slightly downward shift in X:A ratio in ESC, liver cells and brain cells (Fig. 4B). Association of METTL14 is believed to be essential for the METTL3to deposit m6A modification in RNA. Therefore, we analysed the impact of m6A depletion in Mettl14 knockout on the maintenance of an equilibrium X to autosome dosage from available ESC and NPC cell line datasets (Duda et al., 2021; Y. Wang et al., 2018b). Here, we observed a similar scenario where m6A depletion in Mettl14 KO cells only showed a minor downward trend in the X:A ratio compared to WT cells (Fig. 4C). Taken together, our analysis shows that m6A depletion through ablation or KD of m6A-writer enzymes only have minor effects in maintaining X to autosome dosage.

To get a better insight into the essentiality of m6A in the maintenance of optimum X:A dosage, we analysed the change in X:A ratio upon KO of m6A-eraser enzyme FTO. With perturbed m6A-

erasers, autosomal transcripts would be more destabilized compared to X-linked ones, which can affect the overall X to autosomal dosage compensation. Through our analysis, we observed a more-or-less similar X:A ratio in both WT vs. FTO KO cells of the liver and hippocampus (Fig. 4D) (L. Li et al., 2017; Peng et al., 2019). Cumulatively, our analysis suggests that lower m6A enrichment in X-linked transcripts may only have a minor role to play in X-to-autosome dosage compensation.

Discussion

In mammals, males carry heterogametic XY pair while females carry homogametic XX pair of chromosomes. Chromosome-wide inactivation of one out of two female X-chromosomes during early embryonic development, takes care of balancing the sex-specific gene expression imbalance. However, how the expression stoichiometry is maintained between monoallelic X-linked genes and biallelic autosomal genes remained a long-standing question in the field. Comprehensive mapping of the transcriptomic landscape through allele-specific RNA-seq analysis has shown that active-X in males and females undergo upregulation in order to balance the X:AA dosage (Deng et al., 2011; Lentini et al., 2022; Naik et al., 2022). Here, we have dissected the role of m6A RNA methylation in dosage compensation using mouse model. Our study demonstrates that m6A RNA methylation is dispensable for the maintenance of X-linked gene silencing on the inactive-X. However, it has a minor contribution towards the maintenance of X to autosome dosage compensation in a lineage-specific manner.

Currently, RNA-mediated regulation of differential transcript stability of X-chromosome vs. autosomes has been speculated to modulate the transcriptional dosage between monoallelic X-linked genes and biallelic autosomal genes partly (Deng et al., 2013). Here, we have explored whether the relative abundance of m6A on autosomal vs. X-linked transcripts can be linked to the differential transcriptional stability between X-chromosome vs. autosomes. We demonstrate that m6A RNA methylation is always less enriched on the X-linked transcripts compared to the autosomal transcripts in oocyte and early embryonic cells (Zygote, 2-cell, 8-cell, blastocyst, ESC and embryoid bodies) (Fig. 1A and B). The trend of reduced m6A levels on X-chromosomal transcripts was consistent in other cell types such as MEFs, NPCs, MSCs, dendritic cells and liver tissues. Only, cells of different parts of brain did not show much reduction of m6A enrichment on X-linked transcripts compared to the autosomal transcripts. Taken together, we conclude that reduced enrichment of m6A modification on X-linked transcripts compared to the autosomal transcripts is consistent across most of the embryonic or somatic cell types that we have analysed. Indeed, a recent study have shown that preferential destabilization of autosomal transcripts over X-linked transcripts to be the result of higher m6A enrichment on autosomal transcripts in mESCs and different mouse and human tissue types. Moreover, they showed that the X-linked transcripts have evolved to bear lesser m6A motifs and thereby, have lesser m6A enrichment intrinsically compared to autosomal RNAs (Rücklé et al., 2023). Overall, our data support their findings and demonstrate the universality of the observation in different cellular contexts.

Next, we explored the role of m6A RNA methylation in the maintenance of X-linked gene silencing in XEN, EpiSc and TSC cells. Surprisingly, we observed no reactivation of inactivated-X^{Mus}-linked genes upon m6A depletion, suggesting m6A RNA methylation is dispensable for the maintenance of X-linked gene silencing in these cells (Fig. 2 and 3). Previous studies showed that Mettl3 knockout or even segmental deletion of certain m6A-containing sites on *Xist* lncRNA in

mESCs barely abrogates the gene-silencing efficiency during the initiation of XCI (Coker et al., 2020; Nesterova et al., 2019). However, there have been contrasting results in mESCs that show that *XIST* RNA methylation promotes X-linked gene silencing through facilitated binding of several protein complexes involved in gene repression (Patil et al., 2016). Also, work from another group have demonstrated that m6A sites on *XIST* RNA plays a pivotal role in silencing of X-linked genes on the inactive-X in HEK293T cells (Chang et al., 2022). However, a major limitation in both of their study was that they experimented on only a few X-linked genes. Taken together, our study demonstrates that m6A RNA methylation is dispensable for the maintenance of X-linked gene silencing on the inactive-X in XEN, EpiSc and TSC cells. However, one of the limitations of our study is that we performed inhibitor treatment for 12hrs to deplete the m6A level; therefore, in the future, prolonged depletion of m6A may provide better clarity into the requirement of m6A RNA methylation in the maintenance of X-linked gene silencing on the inactive X-chromosome.

Next, we explored if m6A is required for the maintenance of X to autosome dosage compensation. To explore this, we measured the X to autosome gene expression ratio. If m6A-mediated regulation is crucial to maintain the X-to-autosome dosage in cells, perturbation of m6A levels would be expected to cause changes in X:A ratio. We compared the allelic X:A ratio between control and m6A-depleted XEN, TSC and EpiSCs. Our analysis revealed that depletion of global m6A leads to the decrease in active-X^{Mol}:A^{Mol} ratio, suggesting that m6A RNA methylation is important for maintaining the X to autosome dosage in XEN, TSC and EpiSCs (Fig. 4A). Indeed, a recent study has shown that the loss of m6A in ESC and other cell types leads to the reduction in X:A ratio (Ruckle et al. 2023). However, we find that the magnitude of the reduction in X:A ratio upon m6A depletion in XEN, TSC and EpiSCs varied highly. While m6A depleted XEN and TSC showed a slight decrease in X:A ratio, EpiSC showed a significant reduction, suggesting m6A loss impact the X-to autosome dosage compensation in a lineage-specific manner (Fig. 4A). To validate further, we compared the allele-wise expression pattern of autosomal and X-linked gene expression between inhibitor vs. DMSO-treated cells. We found that there were no significant changes in X-linked gene expression between inhibitor and DMSO-treated cells. Interestingly, there were changes in autosomal gene expression between the inhibitor and DMSO-treated cells. Specially, we observed that overall expression of autosomal genes tended to be increased in inhibitor-treated cells compared to the DMSO-treated cells in TSC and EpiSC, suggesting that the loss of m6A destabilizes the X to autosome dosage balance mainly through affecting the autosomal gene expression (Fig. 4A). Separately, although we observed significant global depletion of m6A upon inhibitor treatment for 12hr, we believe a more stringent strategy of prolonged m6A or stable m6A depletion may provide better clarity on the contribution of m6A RNA methylation in the maintenance of X:A dosage compensation in XEN, TSC and EpiSCs. Next, we extended our analysis to different embryonic and somatic cell types. Our analysis revealed that despite the depletion of m6A RNA methylation (~70-99%) in Mettl3 and Mettl14 (m6A-writer) deletion or knockdown cells, there was no significant alteration in the X:A ratio in most of the cases (Fig.4B and C). However, we would like to mention that in many cases, we observed a slight downward shift in X:A ratio in m6A depleted cells. Taken together, we demonstrate that m6A RNA methylation is required but has a minor role in the maintenance of X to autosome dosage compensation. On the other hand, gain of m6A enrichment in FTO (m6A-eraser) knockout hippocampus or liver cells did not alter the X:A ratio. It is worth mentioning that in some of the datasets that we have analysed, we do not have clarity about the efficiency of loss or gain of m6A enrichment such as Mettl3 knockdown in 3T3-L1 MEF cells (Zhao et al., 2014), Mettl14 knockout in RBC ES cell lines (Duda et al., 2021) and FTO knockout in mouse liver (Peng et al., 2019). In

summary, our study provides significant insight into the role of m6A RNA methylation in regulating dosage compensation. We demonstrate that although there is lower m6A-enrichment on X-linked RNAs compared to autosomal transcripts, it is dispensable for the maintenance of XCI, but have a minor contribution towards balancing the X to autosome dosage.

Materials and Methods

Data availability

RNA-seq data generated in this study will be deposited to Gene expression omnibus (GEO) and the reference will be provided upon publication. Details about the previously available dataset have been provided in a supplementary file 1.

Cell culture

XEN cells were cultured on gelatin coated (HiMedia, TCL059) culture dish using Dulbecco's modified eagle medium (DMEM) (HiMedia, AL007A) supplemented with 10% fetal bovine serum (FBS) (Gibco, 10270-106), 75U/ml Penstrep (Gibco, 15070063), 3 mM L-Glutamine (Gibco, 25030081), 1.5X MEM non-essential amino acids (NEAA) (Gibco, 11140-050) and β-Mercaptoethanol (Sigma, M3148).

EpiSCs were cultured on Matrigel (Corning, 354277) coated culture dish using Knock Out DMEM (Gibco. 10829018) supplemented with 20% knock out serum replacement (KSR) (Gibco. 10828028), 75U/ml Penstrep (Gibco, 15070063), 3 mM L-Glutamine (Gibco, 25030081), 1.5X MEM NEAA (Gibco, 11140-050), β-Mercaptoethanol (Sigma, M3148), 10ng/ml Fgf2(Prospect, CYT386) and 20ng/ml Activin A (SinoBiologicals, 10429 HNAH).

TSCs were cultured on gelatin coated culture dish using MEF (mouse embryonic fibroblast) conditioned TSC medium. TSC medium consisted of RPMI (PanBiotech, P04-16500), 2mM L-Glutamine, 50 U/ml Penstrep, 1X MEM NEAA, β-Mercaptoethanol, Sodium Pyruvate. To the finally prepared TSC medium 37.5ng/µl Fgf4 (Peprotech, 45057) was added prior to use. For preparation of MEFconditioned media, MEF cells were cultured with TSC medium in gelatin coated culture dish. All the cell cultures were maintained at 37°C in humid atmosphere with 5% CO2.

METTL3 inhibitor treatment

To inhibit METTL3 in XEN, EpiSCs and TSCs, cells were seeded a day before the treatment. Next day, cells were treated with 50 µM of STM2457 inhibitor (STORM THERAPEUTICs) using the respective culture media for 12 hours. STM2457 inhibitor solution was prepared by dissolving in DMSO (Sigma, A2438). An equivalent volume of DMSO alone was used as a vehicle and treated for 12 hours in parallel to the inhibitor treatment. Following the treatment, cells were harvested in TRIzol reagent (Life technologies 15596-026).

Total RNA isolation

Total RNA from all the cell lines were isolated using TRIzol reagent (Life technologies 15596-026) following manufacturer's instructions and resuspended in ultrapure H2O (Invitrogen, 10977). The concentration and integrity of all the RNA samples were measured and verified in Nanodrop and running on 1% agarose gel respectively.

LC MS/MS

For the liquid chromatography-tandem mass spectrometry (LC-MS/MS) experiment, mRNA from XEN cells, TSCs and EpiSCs were used. First, to remove the genomic DNA contamination, total RNA was treated with Turbo DNase (Invitrogen, AM2238) at 37°C for 45 mins and followed by purified by standard phenol-chloroform isoamyl alcohol method and resuspended in ultrapure H_2O. mRNA was isolated from the DNase-treated total RNA using dynabeads direct mRNA purification kit (Invitrogen, 61011) following the manufacturer's instruction. To prepare the sample for LC-MS/MS, mRNA was hydrolysed in a buffer containing 10U of nuclease P1 (NEB, M0660S), NaCl and ZnCl2 for 2 hours with agitation at 800 rpm for 30s every 5 min at 37°C in thermomixer (Thermofisher), followed by addition of NH4CO3 (Sigma, A6141) and alkaline phosphatase (NEB, M0525S) with additional incubation for 2 hours as before. Tris-HCl was added to stop the reaction and centrifuged at 16000g for 30 mins at 4°C. The supernatant was collected, diluted, and injected into C18 reverse phase column coupled to Shimadzu triple quadrupole (QQQ) mass spectrometer in positive electrospray ionization method. The nucleosides were determined based on the nucleoside to base ion transitions of 268-to-136 for A and 282-to-150 for m6A and quantified from the calibration curve obtained from pure nucleosides of A (Sigma, A9251) and m6A (Abcam, ab145715)) ran at the same batch of samples each time.

RNA sequencing

Total RNA was isolated using TRIzol as mentioned above. RNA quantity was checked on Qubit fluorometer (Thermofisher, Q33238) using RNA HS assay kit (Thermofisher, Q32851) following manufacturer's instruction. The purity and integrity of RNA was checked using Tapestation 4150 using HS RNA screen tape respectively. RNA samples with RIN > 8 were used for the library preparation using TruSeq stranded total RNA kit (Illumina, 15035748). Yield of final prepared libraries were quantified in Qubit 4.0 fluorometer (Thermofisher, Q33238) using DNA HS assay kit (Thermofisher, Q32851) and insert size was determined on Tapestation 4150 (Agilent) using D1000 screentapes (Agilent, 5067-5582). Libraries were finally sequenced on Illumina NovaSeq 6000 platform with paired-end (2 x150) chemistry.

Allele-specific RNA sequencing analysis

Allele-specific expression analysis was performed on the RNA-seq data of XEN, TSCs and EpiSCs. First, we obtained strain-specific SNPs (Mus musculus musculus (Mus) and Mus musculus molossinus (Mol)) from Mouse genome project

(https://www.sanger.ac.uk/science/data/mouse-genomes-project). Next, the variant calling file (VCF) tool was used to create strain-specific in silico reference genomes by incorporating strain-specific SNPs into the mm10 reference genome (Danecek et al., 2011). Next, transcriptomic reads were mapped to the strain-specific reference genome using STAR (--outFilterMultimapNmax 1). Following the mapping of the reads, SNP-wise counts were generated. To remove any false positives in allelic count, SNPs with minimum read counts of 10 per SNP site were only considered. To get the gene wise count, those genes were considered which had at least two such informative SNPs. We calculated allelic read counts for a gene by taking an average of SNP-wise reads. The allelic ratio was calculated using the formula: (Mol-allele or Mus-allele)/(Mol-allele+Mus-allele).

RNA-seq and MeRIP-seq analysis

m6A MeRIP-seq and RNA-seq reads were mapped to mouse reference genome GRCm39 using STAR (v2.7.10a) aligner (Dobin et al., 2013). Gene wise featureCounts (v2.0.1) was used to get counts and normalized to TPM (Liao et al., 2014). Input genes which have >0.5 TPM was used for further analysis to identify m6A enrichment IP over Input and generated log2 (IP TPM/Input TPM +1) values.

X to A ratio

Given the huge differences in the number of genes between X-chromosomes and autosomes, bootstrapping method was considered for profiling the X:A ratio as described previously (Naik et al., 2022; Pacini et al., 2021). For calculating X:A ratio, lowly expressed genes (<5 TPM) were removed from our analysis. Similarly, highly expressed genes were also removed from autosomes and X chromosomes with a 95-percentile threshold for our analysis. To calculate the X:A ratio using the bootstrapping approach, X-linked gene expression (TPM) was divided with the same number of autosomal genes selected randomly and was repeated 1000 times to mitigate a large number of autosomal genes compared to the small number of X chromosomal genes. Finally, X to A ratio was obtained from the median value of 1000 repeats.

Statistical analysis and plots

Plots were generated using R packages ggplot2, Complex Heatmap. For statistical analysis, we used two-sample t-tests and Mann-Whitney U test.

Author's contribution

Conceptualization: SG, HCN, RB and AS. Supervision: SG. Funding: SG. Experiments, data analysis, methodology and resources: HCN, RB, MNM and KS. Writing first draft: AS, RB and HCN. Editing the manuscript: SG, AS, HCN and RB. The final manuscript was approved by all the authors.

Acknowledgement

We thank Prof. Sundeep Kalantry, University of Michigan for providing cell lines used for our experiments in this study. This study is supported by the Department of Biotechnology (DBT), Govt. of India grant (BT/PR30399/BRB/10/1746/2018), DST-SERB (CRG/2019/003067), DBT-Ramalingaswamy fellowship (BT/RLF/Re542 entry/05/2016) and Infosys Young Investigator grant award to SG. RB acknowledge Council of Scientific and Industrial Research (CSIR), India for the fellowship. AS acknowledge MOE for the fellowship.

Conflict of interest

Authors declare no conflict of interest

References

Bachtrog, D. (2013). Y-chromosome evolution: emerging insights into processes of Y-chromosome degeneration. *Nature Reviews. Genetics*, *14*(2), 113–124. https://doi.org/10.1038/NRG3366

Batista, P. J., Molinie, B., Wang, J., Qu, K., Zhang, J., Li, L., Bouley, D. M., Lujan, E., Haddad, B., Daneshvar, K., Carter, A. C., Flynn, R. A., Zhou, C., Lim, K. S., Dedon, P., Wernig, M., Mullen, A. C., Xing, Y., Giallourakis, C. C., & Chang, H. Y. (2014). m6A RNA Modification Controls Cell Fate Transition in Mammalian Embryonic Stem Cells. *Cell Stem Cell*, *15*(6), 707–719. https://doi.org/10.1016/J.STEM.2014.09.019

Berletch, J. B., Yang, F., Xu, J., Carrel, L., & Disteche, C. M. (2011). Genes that escape from X inactivation. *Hum Genet*, *130*, 237–245. https://doi.org/10.1007/s00439-011-1011-z

Berulava, T., Buchholz, E., Elerdashvili, V., Pena, T., Islam, M. R., Lbik, D., Mohamed, B. A., Renner, A., von Lewinski, D., Sacherer, M., Bohnsack, K. E., Bohnsack, M. T., Jain, G., Capece, V., Cleve, N., Burkhardt, S., Hasenfuss, G., Fischer, A., & Toischer, K. (2020). Changes in m6A RNA methylation contribute to heart failure progression by modulating translation. *European Journal of Heart Failure*, *22*(1), 54–66. https://doi.org/10.1002/EJHF.1672

Chang, C., Ma, G., Cheung, E., & Hutchins, A. P. (2022). A programmable system to methylate and demethylate N6-methyladenosine (m6A) on specific RNA transcripts in mammalian

cells. *Journal of Biological Chemistry*, *298*(11), 102525. https://doi.org/10.1016/j.jbc.2022.102525

Charlesworth, B. (1991). The evolution of sex chromosomes. *Science (New York, N.Y.)*, *251*(4997), 1030–1033. https://doi.org/10.1126/science.1998119

Coker, H., Wei, G., Moindrot, B., Mohammed, S., Nesterova, T., & Brockdorff, N. (2020). The role of the Xist 5' m6A region and RBM15 in X chromosome inactivation. *Wellcome Open Research*, *5*, 31. https://doi.org/10.12688/wellcomeopenres.15711.1

Danecek, P., Auton, A., Abecasis, G., Albers, C. A., Banks, E., DePristo, M. A., Handsaker, R. E., Lunter, G., Marth, G. T., Sherry, S. T., McVean, G., & Durbin, R. (2011). The variant call format and VCFtools. *Bioinformatics*, *27*(15), 2156–2158. https://doi.org/10.1093/BIOINFORMATICS/BTR330

Deng, X., Berletch, J. B., Ma, W., Nguyen, D. K., Hiatt, J. B., Noble, W. S., Shendure, J., & Disteche, C. M. (2013). Mammalian X Upregulation Is Associated with Enhanced Transcription Initiation, RNA Half-Life, and MOF-Mediated H4K16 Acetylation. *Developmental Cell*, *25*(1), 55–68. https://doi.org/10.1016/J.DEVCEL.2013.01.028

Deng, X., Hiatt, J. B., Nguyen, D. K., Ercan, S., Sturgill, D., Hillier, L. W., Schlesinger, F., Davis, C. A., Reinke, V. J., Gingeras, T. R., Shendure, J., Waterston, R. H., Oliver, B., Lieb, J. D., & Disteche, C. M. (2011). Evidence for compensatory upregulation of expressed X-linked genes in mammals, Caenorhabditis elegans and Drosophila melanogaster. *Nature Genetics 2011 43:12*, *43*(12), 1179–1185. https://doi.org/10.1038/ng.948

Dobin, A., Davis, C. A., Schlesinger, F., Drenkow, J., Zaleski, C., Jha, S., Batut, P., Chaisson, M., & Gingeras, T. R. (2013). STAR: ultrafast universal RNA-seq aligner. *Bioinformatics*, *29*(1), 15–21. https://doi.org/10.1093/BIOINFORMATICS/BTS635

Dominissini, D., Moshitch-Moshkovitz, S., Schwartz, S., Salmon-Divon, M., Ungar, L., Osenberg, S., Cesarkas, K., Jacob-Hirsch, J., Amariglio, N., Kupiec, M., Sorek, R., & Rechavi, G. (2012). Topology of the human and mouse m6A RNA methylomes revealed by m6A-seq. *Nature 2012 485:7397*, *485*(7397), 201–206. https://doi.org/10.1038/nature11112

Duda, K. J., Ching, R. W., Jerabek, L., Shukeir, N., Erikson, G., Engist, B., Onishi-Seebacher, M., Perrera, V., Richter, F., Mittler, G., Fritz, K., Helm, M., Knuckles, P., Bühler, M., & Jenuwein, T. (2021). m6A RNA methylation of major satellite repeat transcripts facilitates chromatin association and RNA:DNA hybrid formation in mouse heterochromatin. *Nucleic Acids Research*, *49*(10), 5568–5587. https://doi.org/10.1093/nar/gkab364

Gayen, S., Maclary, E., Buttigieg, E., Hinten, M., & Kalantry, S. (2015). A Primary Role for the Tsix lncRNA in Maintaining Random X-Chromosome Inactivation. *Cell Reports*, *11*(8), 1251–1265. https://doi.org/10.1016/J.CELREP.2015.04.039

Gayen, S., Maclary, E., Hinten, M., & Kalantry, S. (2016). Sex-specific silencing of X-linked genes by Xist RNA. *Proceedings of the National Academy of Sciences of the United States of America*, *113*(3), E309–E318. https://doi.org/10.1073/PNAS.1515971113/SUPPL_FILE/PNAS.1515971113.SAPP.PDF

Geula, S., Moshitch-Moshkovitz, S., Dominissini, D., Mansour, A. A. F., Kol, N., Salmon-Divon, M., Hershkovitz, V., Peer, E., Mor, N., Manor, Y. S., Ben-Haim, M. S., Eyal, E., Yunger, S., Pinto, Y., Jaitin, D. A., Viukov, S., Rais, Y., Krupalnik, V., Chomsky, E., … Hanna, J. H. (2015). m6A mRNA methylation facilitates resolution of naïve pluripotency toward differentiation. *Science*, *347*(6225), 1002–1006. https://doi.org/10.1126/SCIENCE.1261417/SUPPL_FILE/1261417TABLES5.XLSX

Harris, C., Cloutier, M., Trotter, M., Hinten, M., Gayen, S., Du, Z., Xie, W., & Kalantry, S. (2019). Conversion of random x-inactivation to imprinted x-inactivation by maternal prc2. *ELife*, *8*. https://doi.org/10.7554/ELIFE.44258

Jia, G., Fu, Y., Zhao, X., Dai, Q., Zheng, G., Yang, Y., Yi, C., Lindahl, T., Pan, T., Yang, Y. G., & He, C. (2011). N6-Methyladenosine in nuclear RNA is a major substrate of the obesity-associated FTO. *Nature Chemical Biology 2011 7:12*, *7*(12), 885–887. https://doi.org/10.1038/nchembio.687

Jiang, X., Liu, B., Nie, Z., Duan, L., Xiong, Q., Jin, Z., Yang, C., & Chen, Y. (2021). The role of m6A modification in the biological functions and diseases. *Signal Transduction and Targeted Therapy*, *6*(1), 74. https://doi.org/10.1038/s41392-020-00450-x

Julien, P., Brawand, D., Soumillon, M., Necsulea, A., Liechti, A., Schütz, F., Daish, T., Grützner, F., & Kaessmann, H. (2012). Mechanisms and Evolutionary Patterns of Mammalian and Avian Dosage Compensation. *PLOS Biology*, *10*(5), e1001328. https://doi.org/10.1371/JOURNAL.PBIO.1001328

Kaur, H., Rv, P., & Gayen, S. (2020). Dampened X-chromosomes in human pluripotent stem cells: dampening or erasure of X-upregulation? *Chromosoma*, *129*(2), 111–113. https://doi.org/10.1007/S00412-019-00717-5/FIGURES/1

Ke, S., Alemu, E. A., Mertens, C., Gantman, E. C., Fak, J. J., Mele, A., Haripal, B., Zucker-Scharff, I., Moore, M. J., Park, C. Y., Vågbø, C. B., Kuśnierczyk, A., Klungland, A., Darnell, J. E., & Darnell, R. B. (2015). A majority of m6A residues are in the last exons, allowing the potential for 3' UTR regulation. *Genes & Development*, *29*(19), 2037–2053. https://doi.org/10.1101/GAD.269415.115

Kharchenko, P. V., Xi, R., & Park, P. J. (2011). Evidence for dosage compensation between the X chromosome and autosomes in mammals. *Nature Genetics*, *43*(12), 1167–1169. https://doi.org/10.1038/NG.991

Knuckles, P., Carl, S. H., Musheev, M., Niehrs, C., Wenger, A., & Bühler, M. (2017). RNA fate determination through cotranscriptional adenosine methylation and microprocessor binding. *Nature Structural & Molecular Biology*, *24*(7), 561–569. https://doi.org/10.1038/NSMB.3419

Lahn, B. T., & Page, D. C. (1999). Four evolutionary strata on the human X chromosome. *Science (New York, N.Y.)*, *286*(5441), 964–967. https://doi.org/10.1126/SCIENCE.286.5441.964

Larsson, A. J. M., Coucoravas, C., Sandberg, R., & Reinius, B. (2019). X-chromosome upregulation is driven by increased burst frequency. *Nature Structural & Molecular Biology*, *26*(10), 963–969. https://doi.org/10.1038/s41594-019-0306-y

Lee, H., Bao, S., Qian, Y., Geula, S., Leslie, J., Zhang, C., Hanna, J. H., & Ding, L. (2019). Stage-specific requirement for Mettl3-dependent m6A mRNA methylation during haematopoietic stem cell differentiation. *Nature Cell Biology 2019 21:6*, *21*(6), 700–709. https://doi.org/10.1038/s41556-019-0318-1

Lentini, A., Cheng, H., Noble, J. C., Papanicolaou, N., Coucoravas, C., Andrews, N., Deng, Q., Enge, M., & Reinius, B. (2022). Elastic dosage compensation by X-chromosome upregulation. *Nature Communications*, *13*(1), 1854. https://doi.org/10.1038/s41467-022-29414-1

Li, H. B., Tong, J., Zhu, S., Batista, P. J., Duffy, E. E., Zhao, J., Bailis, W., Cao, G., Kroehling, L., Chen, Y., Wang, G., Broughton, J. P., Chen, Y. G., Kluger, Y., Simon, M. D., Chang, H. Y., Yin, Z., & Flavell, R. A. (2017). m6A mRNA methylation controls T cell homeostasis by targeting the IL-7/STAT5/SOCS pathways. *Nature 2017 548:7667*, *548*(7667), 338–342. https://doi.org/10.1038/nature23450

Li, L., Zang, L., Zhang, F., Chen, J., Shen, H., Shu, L., Liang, F., Feng, C., Chen, D., Tao, H., Xu, T., Li, Z., Kang, Y., Wu, H., Tang, L., Zhang, P., Jin, P., Shu, Q., & Li, X. (2017). Fat mass and obesity-associated (FTO) protein regulates adult neurogenesis. *Human Molecular Genetics*, *26*(13), 2398–2411. https://doi.org/10.1093/hmg/ddx128

Li, Y., Xia, L., Tan, K., Ye, X., Zuo, Z., Li, M., Xiao, R., Wang, Z., Liu, X., Deng, M., Cui, J., Yang, M., Luo, Q., Liu, S., Cao, X., Zhu, H., Liu, T., Hu, J., Shi, J., … Xia, L. (2020). N6-Methyladenosine co-transcriptionally directs the demethylation of histone H3K9me2. *Nature Genetics 2020 52:9*, *52*(9), 870–877. https://doi.org/10.1038/s41588-020-0677-3

Liao, Y., Smyth, G. K., & Shi, W. (2014). featureCounts: an efficient general purpose program for assigning sequence reads to genomic features. *Bioinformatics*, *30*(7), 923–930. https://doi.org/10.1093/BIOINFORMATICS/BTT656

Liu, J., Yue, Y., Han, D., Wang, X., Fu, Y., Zhang, L., Jia, G., Yu, M., Lu, Z., Deng, X., Dai, Q., Chen, W., & He, C. (2013). A METTL3–METTL14 complex mediates mammalian nuclear RNA N6-adenosine methylation. *Nature Chemical Biology 2013 10:2*, *10*(2), 93–95. https://doi.org/10.1038/nchembio.1432

Livernois, A. M., Graves, J. A. M., & Waters, P. D. (2012). The origin and evolution of vertebrate sex chromosomes and dosage compensation. *Heredity*, *108*(1), 50–58. https://doi.org/10.1038/hdy.2011.106

Lyon, M. F. (1961). Gene action in the X-chromosome of the mouse (mus musculus L.). *Nature*, *190*(4773), 372–373. https://doi.org/10.1038/190372A0

Maclary, E., Buttigieg, E., Hinten, M., Gayen, S., Harris, C., Sarkar, M. K., Purushothaman, S., & Kalantry, S. (2014). Differentiation-dependent requirement of Tsix long non-coding RNA in imprinted X-chromosome inactivation. *Nature Communications 2014 5:1*, *5*(1), 1–14. https://doi.org/10.1038/ncomms5209

Marshall Graves, J. A. (2015). Evolution of vertebrate sex chromosomes and dosage compensation. *Nature Publishing Group*. https://doi.org/10.1038/nrg.2015.2

Meyer, K. D., Saletore, Y., Zumbo, P., Elemento, O., Mason, C. E., & Jaffrey, S. R. (2012). Comprehensive Analysis of mRNA Methylation Reveals Enrichment in 3′ UTRs and near Stop Codons. *Cell*, *149*(7), 1635–1646. https://doi.org/10.1016/J.CELL.2012.05.003

Naik, H. C., Hari, K., Chandel, D., Jolly, M. K., & Gayen, S. (2022). Single-cell analysis reveals X upregulation is not global in pre-gastrulation embryos. *IScience*, *25*(6). https://doi.org/10.1016/J.ISCI.2022.104465

Nesterova, T. B., Wei, G., Coker, H., Pintacuda, G., Bowness, J. S., Zhang, T., Almeida, M., Bloechl, B., Moindrot, B., Carter, E. J., Alvarez Rodrigo, I., Pan, Q., Bi, Y., Song, C. X., & Brockdorff, N. (2019). Systematic allelic analysis defines the interplay of key pathways in X chromosome inactivation. *Nature Communications*, *10*(1). https://doi.org/10.1038/S41467-019-11171-3

Ohno, S. (1967). *Sex Chromosomes and Sex-Linked Genes*. *1*. https://doi.org/10.1007/978-3-642-88178-7

Pacini, G., Dunkel, I., Mages, N., Mutzel, V., Timmermann, B., Marsico, A., & Schulz, E. G. (2021). Integrated analysis of Xist upregulation and X-chromosome inactivation with single-cell and single-allele resolution. *Nature Communications*, *12*(1). https://doi.org/10.1038/S41467-021-23643-6

Patil, D. P., Chen, C. K., Pickering, B. F., Chow, A., Jackson, C., Guttman, M., & Jaffrey, S. R. (2016). m6A RNA methylation promotes XIST-mediated transcriptional repression. *Nature 2016 537:7620*, *537*(7620), 369–373. https://doi.org/10.1038/nature19342

Peng, S., Xiao, W., Ju, D., Sun, B., Hou, N., Liu, Q., Wang, Y., Zhao, H., Gao, C., Zhang, S., Cao, R., Li, P., Huang, H., Ma, Y., Wang, Y., Lai, W., Ma, Z., Zhang, W., Huang, S., … Huang, N. (2019). Identification of entacapone as a chemical inhibitor of FTO mediating metabolic regulation through FOXO1. *Science Translational Medicine*, *11*(488), 7116. https://doi.org/10.1126/SCITRANSLMED.AAU7116/SUPPL_FILE/AAU7116_SM.PDF

Ping, X. L., Sun, B. F., Wang, L., Xiao, W., Yang, X., Wang, W. J., Adhikari, S., Shi, Y., Lv, Y., Chen, Y. S., Zhao, X., Li, A., Yang, Y., Dahal, U., Lou, X. M., Liu, X., Huang, J., Yuan, W. P., Zhu, X. F., … Yang, Y. G. (2014). Mammalian WTAP is a regulatory subunit of the RNA N6-methyladenosine methyltransferase. *Cell Research 2014 24:2*, *24*(2), 177–189. https://doi.org/10.1038/cr.2014.3

Pupak, A., Singh, A., Sancho-Balsells, A., Alcalá-Vida, R., Marc Espina, ·, Giralt, A., Martí, E., Andersson, U., Ørom, V., Ginés, · Silvia, & Brito, V. (2022). Altered m6A RNA methylation contributes to hippocampal memory deficits in Huntington's disease mice. *Cellular and Molecular Life Sciences*, *79*, 416. https://doi.org/10.1007/s00018-022-04444-6

Roundtree, I. A., Evans, M. E., Pan, T., & He, C. (2017). Dynamic RNA Modifications in Gene Expression Regulation. *Cell*, *169*(7), 1187–1200. https://doi.org/10.1016/J.CELL.2017.05.045

Rücklé, C., Körtel, N., Basilicata, M. F., Busch, A., Zhou, Y., Hoch-Kraft, P., Tretow, K., Kielisch, F., Bertin, M., Pradhan, M., Musheev, M., Schweiger, S., Niehrs, C., Rausch, O., Zarnack, K., Keller Valsecchi, C. I., & König, J. (2023). RNA stability controlled by m6A methylation contributes to X-to-autosome dosage compensation in mammals. *Nature Structural & Molecular Biology*. https://doi.org/10.1038/s41594-023-00997-7

Sarkar, M. K., Gayen, S., Kumar, S., Maclary, E., Buttigieg, E., Hinten, M., Kumari, A., Harris, C., Sado, T., & Kalantry, S. (2015). An Xist-activating antisense RNA required for X-chromosome inactivation. *Nature Communications 2015 6:1*, *6*(1), 1–13. https://doi.org/10.1038/ncomms9564

Selmi, T., & Lanzuolo, C. (2022). Driving Chromatin Organisation through N6-methyladenosine Modification of RNA: What Do We Know and What Lies Ahead? *Genes 2022, Vol. 13, Page 340*, *13*(2), 340. https://doi.org/10.3390/GENES13020340

Shi, H., Wang, X., Lu, Z., Zhao, B. S., Ma, H., Hsu, P. J., Liu, C., & He, C. (2017). YTHDF3 facilitates translation and decay of N6-methyladenosine-modified RNA. *Cell Research 2017 27:3*, *27*(3), 315–328. https://doi.org/10.1038/cr.2017.15

Slobodin, B., Han, R., Calderone, V., Vrielink, J. A. F. O., Loayza-Puch, F., Elkon, R., & Agami, R. (2017). Transcription Impacts the Efficiency of mRNA Translation via Co-transcriptional N6-adenosine Methylation. *Cell*, *169*(2), 326-337.e12. https://doi.org/10.1016/J.CELL.2017.03.031

Talon, I., Janiszewski, A., Theeuwes, B., Lefevre, T., Song, J., Bervoets, G., Vanheer, L., De Geest, N., Poovathingal, S., Allsop, R., Marine, J. C., Rambow, F., Voet, T., & Pasque, V. (2021). Enhanced chromatin accessibility contributes to X chromosome dosage compensation in mammals. *Genome Biology 2021 22:1*, *22*(1), 1–36. https://doi.org/10.1186/S13059-021-02518-5

Wang, C.-X., Cui, G.-S., Liu, X., Xu, K., Wang, M., Zhang, X.-X., Jiang, L.-Y., Li, A., Yang, Y., Lai, W.-Y., Sun, B.-F., Jiang, G.-B., Wang, H.-L., Tong, W.-M., Li, W., Wang, X.-J., Yang, Y.-G., & Zhou, Q. (2018). METTL3-mediated m6A modification is required for cerebellar development. *PLOS Biology*, *16*(6), e2004880. https://doi.org/10.1371/journal.pbio.2004880

Wang, H., Hu, X., Huang, M., Liu, J., Gu, Y., Ma, L., Zhou, Q., & Cao, X. (2019). Mettl3-mediated mRNA m6A methylation promotes dendritic cell activation. *Nature Communications*, *10*(1), 1898. https://doi.org/10.1038/s41467-019-09903-6

Wang, S., Chen, S., Sun, J., Han, P., Xu, B., Li, X., Zhong, Y., Xu, Z., Zhang, P., Mi, P., Zhang, C., Li, L., Zhang, H., Xia, Y., Li, S., Heikenwalder, M., & Yuan, D. (2023). m6A modification-tuned sphingolipid metabolism regulates postnatal liver development in male mice. *Nature Metabolism*, *5*(5), 842–860. https://doi.org/10.1038/s42255-023-00808-9

Wang, X., Lu, Z., Gomez, A., Hon, G. C., Yue, Y., Han, D., Fu, Y., Parisien, M., Dai, Q., Jia, G., Ren, B., Pan, T., & He, C. (2013). N6-methyladenosine-dependent regulation of messenger RNA stability. *Nature 2013 505:7481*, *505*(7481), 117–120. https://doi.org/10.1038/nature12730

Wang, X., Zhao, B. S., Roundtree, I. A., Lu, Z., Han, D., Ma, H., Weng, X., Chen, K., Shi, H., & He, C. (2015). N6-methyladenosine Modulates Messenger RNA Translation Efficiency. *Cell*, *161*(6), 1388–1399. https://doi.org/10.1016/J.CELL.2015.05.014

Wang, Y., Li, Y., Yue, M., Wang, J., Kumar, S., Wechsler-Reya, R. J., Zhang, Z., Ogawa, Y., Kellis, M., Duester, G., & Zhao, J. C. (2018). N6-methyladenosine RNA modification regulates embryonic neural stem cell self-renewal through histone modifications. *Nature Neuroscience 2018 21:2*, *21*(2), 195–206. https://doi.org/10.1038/s41593-017-0057-1

Wei, J., Yu, X., Yang, L., Liu, X., Gao, B., Huang, B., Dou, X., Liu, J., Zou, Z., Cui, X. L., Zhang, L. S., Zhao, X., Liu, Q., He, P. C., Sepich-Poore, C., Zhong, N., Liu, W., Li, Y., Kou, X., … He, C. (2022). FTO mediates LINE1 m6A demethylation and chromatin regulation in mESCs and mouse development. *Science (New York, N.Y.)*, *376*(6596). https://doi.org/10.1126/SCIENCE.ABE9582

Wu, Y., Xie, L., Wang, M., Xiong, Q., Guo, Y., Liang, Y., Li, J., Sheng, R., Deng, P., Wang, Y., Zheng, R., Jiang, Y., Ye, L., Chen, Q., Zhou, X., Lin, S., & Yuan, Q. (2018). Mettl3-mediated m6A RNA methylation regulates the fate of bone marrow mesenchymal stem cells and osteoporosis. *Nature Communications*, *9*(1), 4772. https://doi.org/10.1038/s41467-018-06898-4

Xiao, W., Adhikari, S., Dahal, U., Chen, Y. S., Hao, Y. J., Sun, B. F., Sun, H. Y., Li, A., Ping, X. L., Lai, W. Y., Wang, X., Ma, H. L., Huang, C. M., Yang, Y., Huang, N., Jiang, G. Bin, Wang, H. L., Zhou, Q., Wang, X. J., … Yang, Y. G. (2016). Nuclear m6A Reader YTHDC1 Regulates mRNA Splicing. *Molecular Cell*, *61*(4), 507–519. https://doi.org/10.1016/J.MOLCEL.2016.01.012

Xiong, Y., Chen, X., Chen, Z., Wang, X., Shi, S., Wang, X., Zhang, J., & He, X. (2010). RNA sequencing shows no dosage compensation of the active X-chromosome. *Nature Genetics*, *42*(12), 1043–1047. https://doi.org/10.1038/ng.711

Xu, W., Li, J., He, C., Wen, J., Ma, H., Rong, B., Diao, J., Wang, L., Wang, J., Wu, F., Tan, L., Shi, Y. G., Shi, Y., & Shen, H. (2021). METTL3 regulates heterochromatin in mouse embryonic stem cells. *Nature 2021 591:7849*, *591*(7849), 317–321. https://doi.org/10.1038/s41586-021-03210-1

Yankova, E., Blackaby, W., Albertella, M., Rak, J., De Braekeleer, E., Tsagkogeorga, G., Pilka, E. S., Aspris, D., Leggate, D., Hendrick, A. G., Webster, N. A., Andrews, B., Fosbeary, R., Guest, P., Irigoyen, N., Eleftheriou, M., Gozdecka, M., Dias, J. M. L., Bannister, A. J., … Kouzarides, T. (2021). Small-molecule inhibition of METTL3 as a strategy against myeloid leukaemia. *Nature 2021 593:7860*, *593*(7860), 597–601. https://doi.org/10.1038/s41586-021-03536-w

Zaccara, S., & Jaffrey, S. R. (2020). A Unified Model for the Function of YTHDF Proteins in Regulating m6A-Modified mRNA. *Cell*, *181*(7), 1582-1595.e18. https://doi.org/10.1016/J.CELL.2020.05.012

Zhao, X., Yang, Y., Sun, B.-F., Shi, Y., Yang, X., Xiao, W., Hao, Y.-J., Ping, X.-L., Chen, Y.-S., Wang, W.-J., Jin, K.-X., Wang, X., Huang, C.-M., Fu, Y., Ge, X.-M., Song, S.-H., Jeong, H. S., Yanagisawa, H., Niu, Y., … Yang, Y.-G. (2014). FTO-dependent demethylation of N6-methyladenosine regulates mRNA splicing and is required for adipogenesis. *Cell Research*, *24*(12), 1403–1419. https://doi.org/10.1038/cr.2014.151

Zheng, G., Dahl, J. A., Niu, Y., Fedorcsak, P., Huang, C. M., Li, C. J., Vågbø, C. B., Shi, Y., Wang, W. L., Song, S. H., Lu, Z., Bosmans, R. P. G., Dai, Q., Hao, Y. J., Yang, X., Zhao, W. M., Tong, W. M., Wang, X. J., Bogdan, F., … He, C. (2013). ALKBH5 Is a Mammalian RNA Demethylase that Impacts RNA Metabolism and Mouse Fertility. *Molecular Cell*, *49*(1), 18–29. https://doi.org/10.1016/J.MOLCEL.2012.10.015

Fig. 1

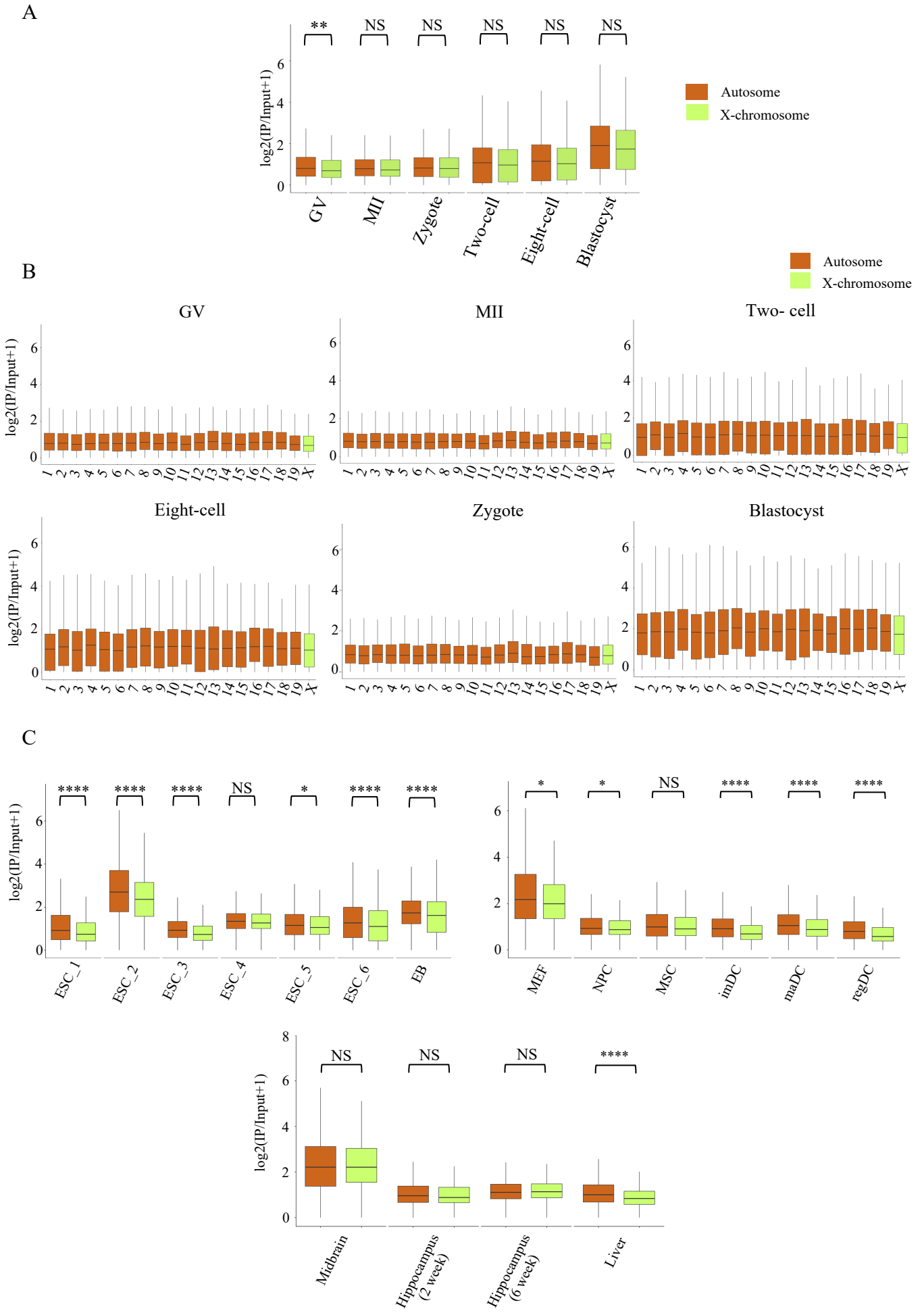
A
log2(IP/Input+1)
**
NS
NS
NS
NS
NS
GV
MII
Zygote
Two-cell
Eight-cell
Blastocyst
Autosome
X-chromosome
B
Autosome
X-chromosome
GV
MII
Two- cell
Eight-cell
Zygote
Blastocyst
log2(IP/Input+1)
1 2 3 4 5 6 7 8 9 10 11 12 13 14 15 16 17 18 19 X
C
log2(IP/Input+1)
****
****
****
NS
*
****
****
ESC_1
ESC_2
ESC_3
ESC_4
ESC_5
ESC_6
EB
*
*
NS
****
****
****
MEF
NPC
MSC
imDC
maDC
regDC
NS
NS
NS
****
Midbrain
Hippocampus (2 week)
Hippocampus (6 week)
Liver

Fig.1: Comparison of m6A enrichment between autosomal versus X-chromosomal transcripts in different cell types and tissues. (A) RNA m6A enrichment autosomes vs. X-linked transcripts in mouse oocyte and different stages of early embryonic development. Edges of each box represents 25th and 75th quartiles and center line denotes the median value; Mann-Whitney U test; ** P value < 0.01; GV- germinal vesicle stage oocyte, MII- metaphase II stage oocyte. (B) RNA m6A enrichment is shown for the transcripts of each autosome and X-chromosome in mouse oocytes and different stages of early embryonic development. (C) Autosome vs X-chromosomal transcripts RNA m6A enrichment among different mouse embryonic stem cell lines (left), different cell types (right) and tissues (bottom). Mann-Whitney U test , *P value < 0.01, ****P value < 0.0001, NS- nonsignificant; MEF- mouse embryonic fibroblasts, NPC- neural progenitor cells, MSC- mesenchymal stem cells, maDC-mature dendritic cells, imDC-immature dendritic cells, regDC-regulatory dendritic cells.

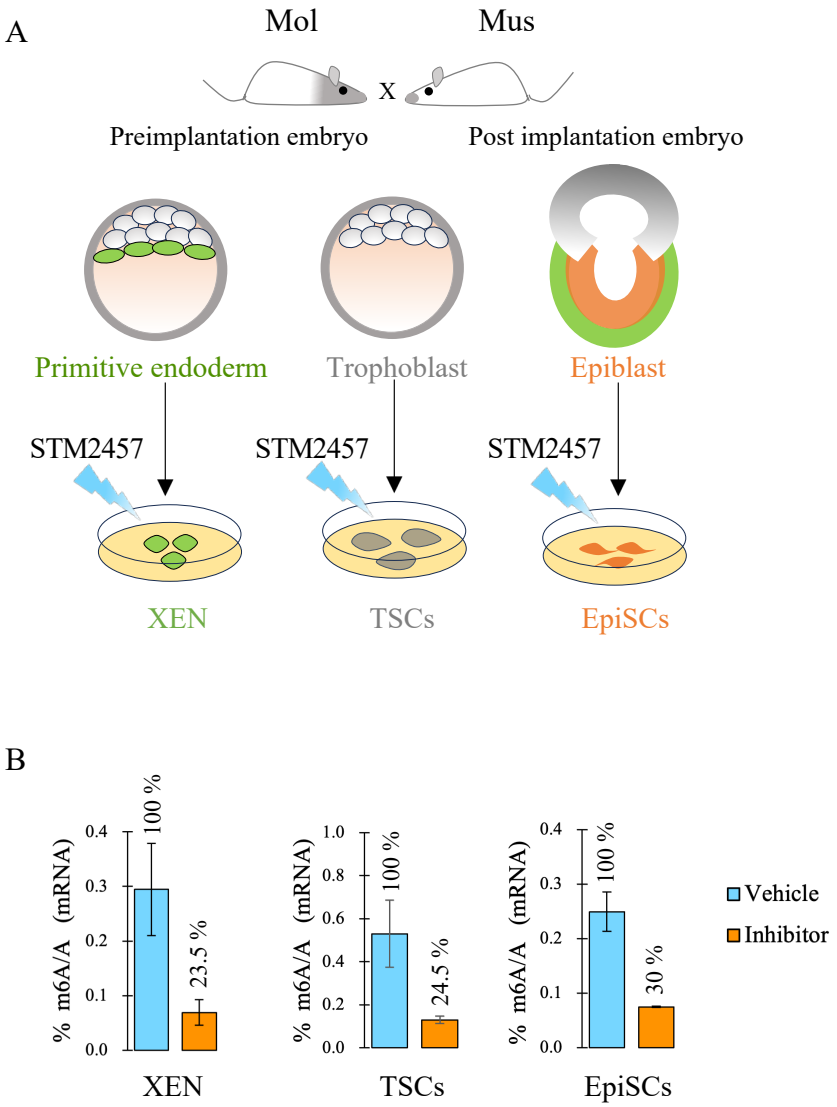
A
Mol
Mus
x
Preimplantation embryo
Post implantation embryo
Primitive endoderm
Trophoblast
Epiblast
STM2457
STM2457
STM2457
XEN
TSCs
EpiSCs
B
% m6A/A (mRNA)
0.0
0.1
0.2
0.3
0.4
100 %
23.5 %
XEN
% m6A/A (mRNA)
0.0
0.2
0.4
0.6
0.8
1.0
100 %
24.5 %
TSCs
% m6A/A (mRNA)
0.0
0.1
0.2
0.3
0.4
100 %
30 %
EpiSCs
Vehicle
Inhibitor

Fig. 2: Inhibition of METTL3 reduces RNA m6A levels in XEN, TSCs and EpiSC. (A) Diagrammatic representation showing METTL3 inhibitor (STM2457) treatment in XEN, TSCs and EpiSCs originating from its precursor cells during mouse early embryo development. (B) Quantification of m6A levels relative to A in mRNAs of XEN cells, EpiSCs and TSCs by liquid chromatography-tandem mass spectrometry (LC-MS/MS) upon METTL3 inhibitor (STM2457, 50μM) and vehicle (DMSO) treatment for 12 hrs. Error bar represents standard deviation of mean for XEN, n=3, TSCs, n=2 and EpiSCs, n=2; XEN – extraembryonic endoderm cells, TSC – trophoblast stem cells, EpiSC – epiblast stem cells.

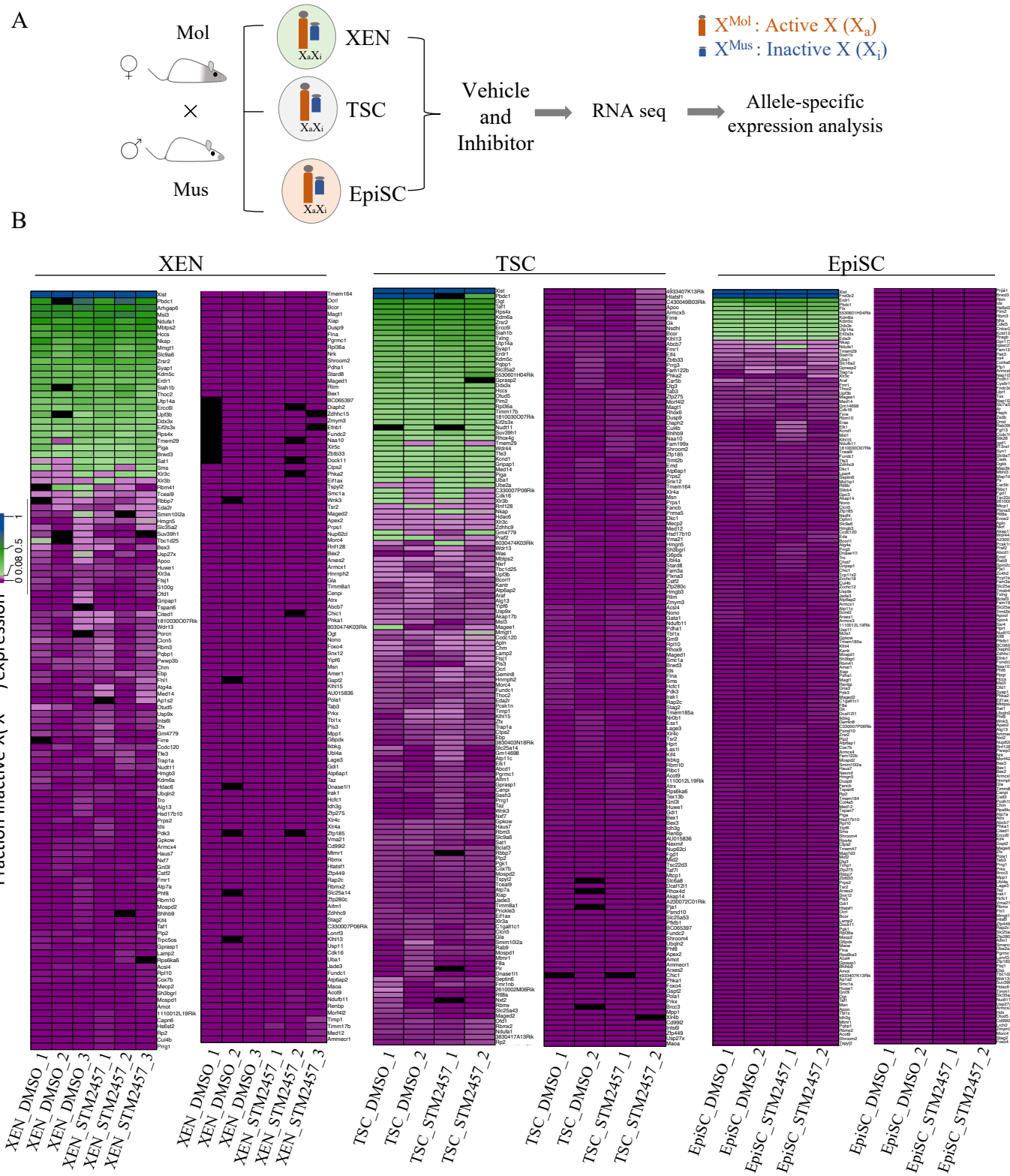
A
Mol
Mus
XEN
TSC
EpiSC
XaXi
Vehicle and Inhibitor
RNA seq
Allele-specific expression analysis
XMol : Active X (Xa)
XMus : Inactive X (Xi)
B
XEN
TSC
EpiSC
Fraction inactive-X(XMus) expression
XEN_DMSO_1
XEN_DMSO_2
XEN_DMSO_3
XEN_STM2457_1
XEN_STM2457_2
XEN_STM2457_3
TSC_DMSO_1
TSC_DMSO_2
TSC_STM2457_1
TSC_STM2457_2
EpiSC_DMSO_1
EpiSC_DMSO_2
EpiSC_STM2457_1
EpiSC_STM2457_2

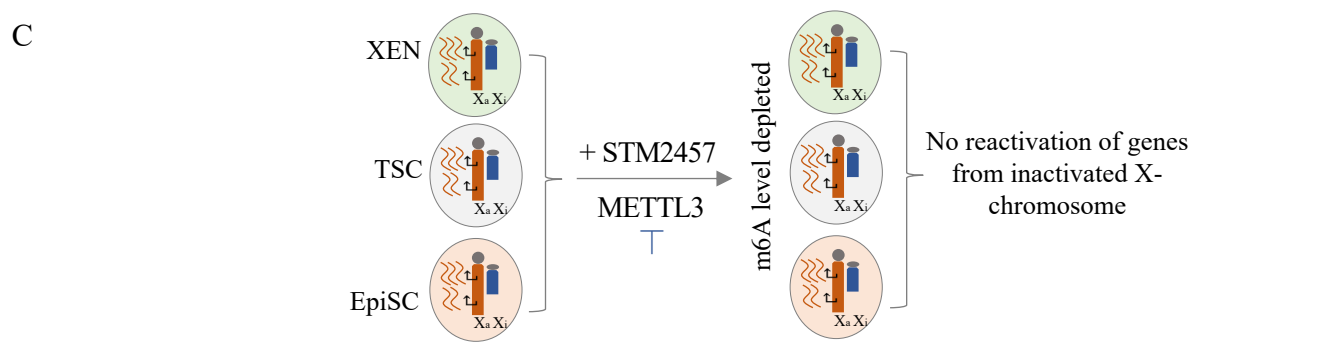
C
XEN
TSC
EpiSC
Xa Xi
+ STM2457
METTL3
m6A level depleted
No reactivation of genes from inactivated X-chromosome

Fig.3: Depletion of RNA m6A level does not affect the expression of genes from inactivated X-chromosome. (A) Schematic outline showing allelic RNA-seq analysis in vehicle and METTL3 inhibitor-treated XEN, TSCs and EpiSCs. These cells are hybrid cells and have polymorphic X-chromosomes which facilitates allele-specific expression analysis of X- linked genes from active vs. inactive X-chromosome. In all the cell lines, X-chromosome from *Mus musculus* origin (X^{Mus}) represents the inactive-X and X-chromosome from *Mus molossinus* origin (X^{Mol}) represents active-X. (B)Heat map showing the fraction allelic expression of X-linked genes from the inactive-X chromosome (X^{Mus}) in vehicle vs. METTL3 inhibitor treated XEN, TSCs and EpiSCss. (C) Schematic diagram showing depletion of RNA m6A level has no effect on X-linked gene silencing from inactivated X- chromosome; XEN – extraembryonic endoderm cells, TSCs – trophoblast stem cells, EpiSCs – epiblast stem cells.

A

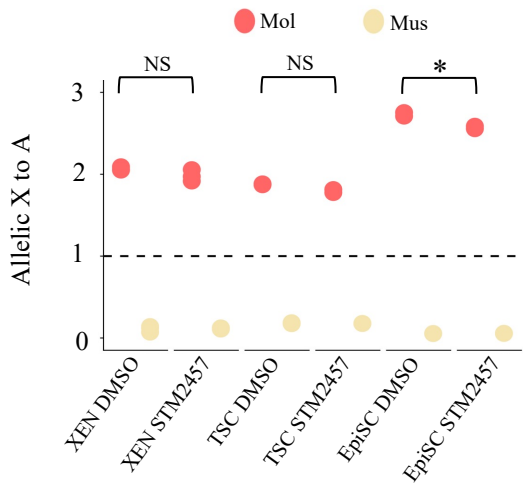
Mol
Mus
Allelic X to A
NS
NS
*
XEN DMSO
XEN STM2457
TSC DMSO
TSC STM2457
EpiSC DMSO
EpiSC STM2457

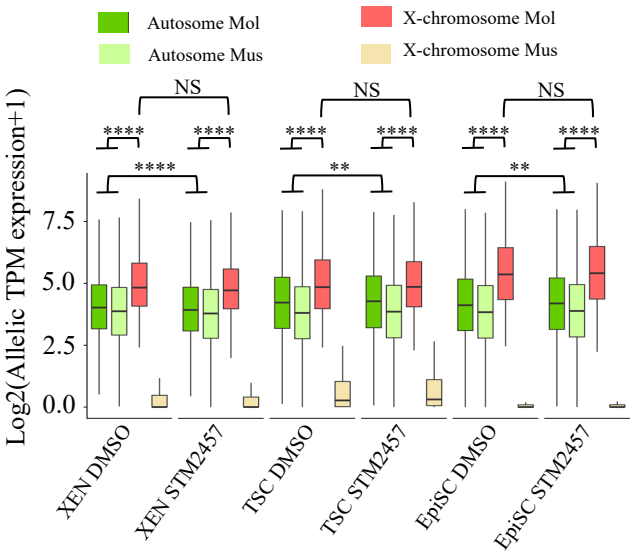
Autosome Mol
Autosome Mus
X-chromosome Mol
X-chromosome Mus
Log2(Allelic TPM expression+1)
NS
****
**
XEN DMSO
XEN STM2457
TSC DMSO
TSC STM2457
EpiSC DMSO
EpiSC STM2457

B

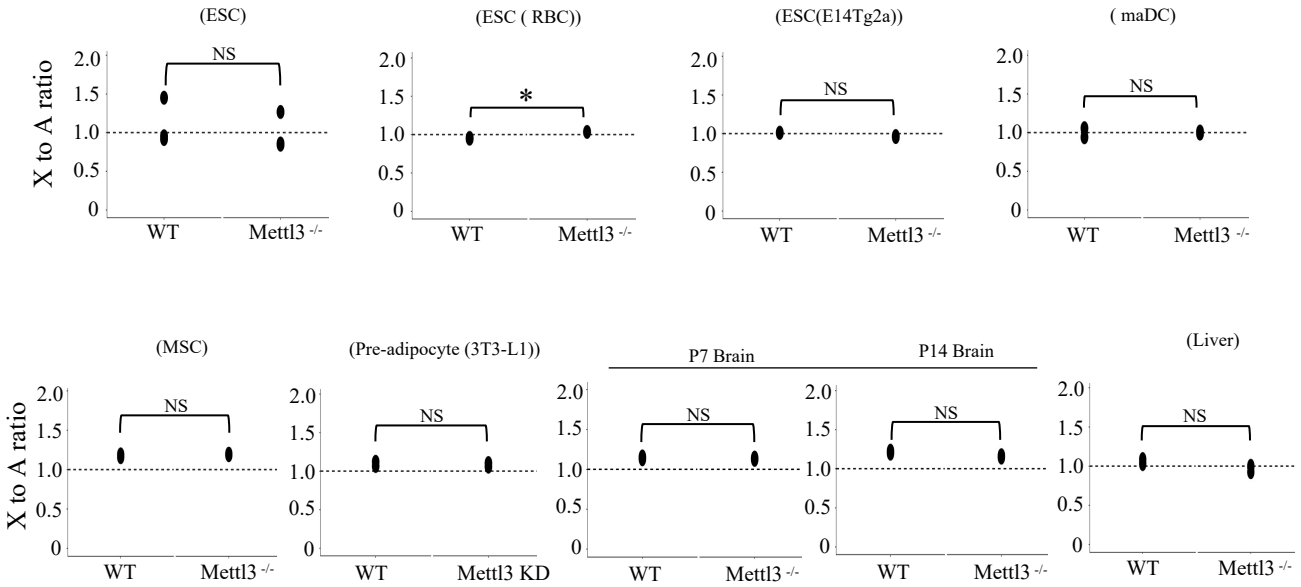
(ESC)
(ESC (RBC))
(ESC(E14Tg2a))
(maDC)
(MSC)
(Pre-adipocyte (3T3-L1))
P7 Brain
P14 Brain
(Liver)
X to A ratio
NS
*
WT
Mettl3 -/-
Mettl3 KD

C

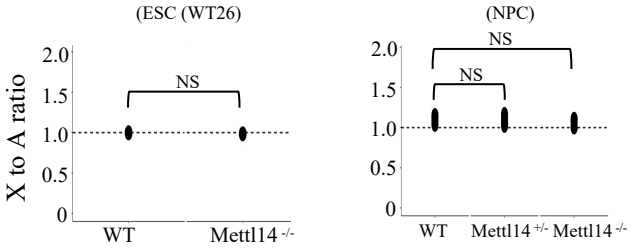
(ESC (WT26)
(NPC)
X to A ratio
NS
WT
Mettl14 -/-
Mettl14 +/-

D

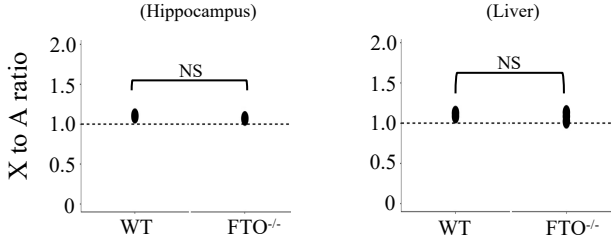
(Hippocampus)
(Liver)
X to A ratio
NS
WT
FTO-/-

Fig.4: Effect of depletion of RNA m6A levels on X to autosome dosage maintenance. (A) Allelic X:A ratio of genes expressed from X-chromosome and autosomes in vehicle (DMSO) vs. METTL3 inhibitor (STM2457) treated XEN, TSCs and EpiSCs (left); Two sample t- test; *P value < 0.05; NS-nonsignificant. Boxplot showing allelic expression of autosomal and X-linked genes in vehicle and METTL3 inhibitor treated XEN, TSCs and EpiSCs (right); Mann-Whitney U test; *P value < 0.05, ** P value < 0.01 , ****P value < 0.0001; NS – nonsignificant. *(*B) Comparison of X:A ratio between WT and Mettl3 KO or KD cells; Two sample t- test; *P value < 0.05; NS – nonsignificant.. (C) Comparison of X:A ratio between WT and Mettl14 KO cells; Two sample t- test; NS – nonsignificant. (D) Comparison of X:A ratio between WT and FTO KO tissues; Two sample t- test; NS – nonsignificant.